ACS APPLIED ENERGY MATERIALS

www.acsaem.org

Article

Understanding Lithium-Ion Conductivity in NASICON-Type Polymer-in-Ceramic Composite Electrolytes

Funeka P. Nkosi, Ignacio Cuevas, Mario Valvo,* Jonas Mindemark, Andrii Mahun, Sabina Abbrent, Jiří Brus, Libor Kobera, and Kristina Edström

Cite This: *ACS Appl. Energy Mater.* 2024, 7, 4609−4619

Read Online

ACCESS | Metrics & More | Article Recommendations | Supporting Information

ABSTRACT: Composite electrolytes comprising distinctive polyether (PEO) or polyester (PCL, P(CL-*co*-TMC)) polymers in combination with a high loading of $Li_{1.4}Al_{0.4}Ti_{1.6}(PO_4)_3$ NASICON-type ceramic powders (LATP, 70 wt %) are investigated to gain insights into the limitations of their ion conductivity in resulting polymer-in-ceramic solid-state electrolyte systems. Here, LATP constitutes an advantageous ceramic Li-ion conductor with fair ionic conductivity that does not immediately suffer from limitations arising from interface issues due to the detrimental formation of surface species (e.g., Li_2CO_3) in contact with air and/or surrounding polymers. The Li-ion transport in all these composite electrolytes is found to follow a slow-motion regime in the polymer matrix, regardless of the nature of the polymer used. Interestingly, the weakly Li-coordinating polyester-based polymers PCL and P(CL-*co*-TMC) exhibit an exchange of Li^+ ions between the polymer and ceramic phases and high Li-ion transference numbers compared to the polyether PEO matrix, which has strong Li−polymer coordination. LATP particle agglomeration is nevertheless observed in all the composite electrolytes, and this most likely represents a dominating cause for the lower Li-ion conductivity values of these composites when compared to those of their solid polymer electrolyte (SPE) counterparts. These findings add another step toward the development of functional composite electrolytes for all-solid-state batteries.

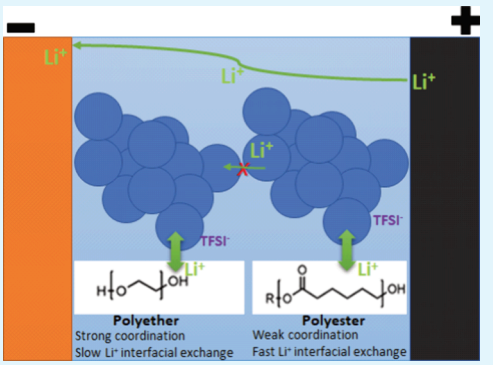

KEYWORDS: *$Li_{1+x}Al_xTi_{2-x}(PO_4)_3$, All-solid-state batteries, Polyether and polyester polymers, Li-ion coordination properties, Interfacial Li-ion transport*

1. INTRODUCTION

Polymer−ceramic composite electrolytes (CPEs) are an attractive type of solid-state electrolyte because they provide a range of characteristic properties of polymer and ceramic electrolyte materials. As such, composite electrolytes with high ceramic loadings typically possess good mechanical strength as well as higher electrochemical and thermal stability compared to those provided by their solid polymer electrolyte (SPE) equivalents. Polymer-in-ceramic composite electrolytes are therefore promising to advance the electrochemical performance of all-solid-state lithium batteries and have gained significant attention due the current demand of high energy density and safe batteries.[1,2]

In CPEs with high ceramic loadings, i.e., polymer-in-ceramic electrolytes, the SPE matrix exhibits a series of key functions: (i) it acts as a multipurpose binder to glue the ceramic particles together, obviating the high grain boundary resistance and possible formation of lithium dendrites at the grain boundaries. (ii) It introduces additional Li-ion transport pathways. (iii) It enhances the flexibility of the corresponding electrolytes, and (iv) it sensibly improves the processability of the entire solid electrolyte, avoiding problematic high-temperature sintering often required to densify the ceramic electrolytes.

Polymer-in-ceramic CPEs potentially possess multiple Li-ion transport pathways inclusive of the ceramic fillers, polymer matrix, and associated polymer−ceramic interface and/or interphases. These different pathways for Li^+ ions, in turn, influence the total ionic conductivity of the resulting composite electrolytes. Attaining a high ionic conductivity for polymer-in-ceramic electrolytes without compromising their mechanical and processability features is crucial for a full utilization of solid-state lithium batteries (SSLBs) and represents one of the major issues currently halting the ultimate performance of these types of electrolytes, making them often not competitive with respect to their liquid counterparts.

Scarce progress has been made so far in the literature to investigate the Li-ion conductivity in composite electrolytes and the aspects limiting its ultimate values. According to Guo et al., an interface is intrinsically formed between the ceramic

Received: March 20, 2024
Revised: May 7, 2024
Accepted: May 8, 2024
Published: May 13, 2024

https://doi.org/10.1021/acsaem.4c00701
ACS Appl. Energy Mater. 2024, 7, 4609−4619

and the polymer matrix, which gives rise to an amorphous space charge region that consists of a redistribution of lithium vacancies and Li^+ ions.[3] In the presence of the polymer matrix, the Li^+ ions in the ceramic particles move to their surface, thus leaving behind lithium vacancies in the ceramic bulk because of the polymer matrix exerting a stabilizing effect in drawing the Li^+ ions from the ceramic lattice toward the associated ceramic surface.[3] Ganesan et al. studied various polymer−ceramic composite systems using molecular dynamics (MD) simulations and found that the ceramic particles slow the dynamics of polymer segments near their surfaces, i.e., at the ceramic−polymer interface.[4,5] Furthermore, Chen et al. revealed that there is a change of the polymer dynamics at this interface influenced by the presence of lithium salt.[6] In the absence of a lithium salt, such as lithium bis(trifluoromethanesulfonyl)-imide (LiTFSI), the ceramic caused a negligible change in the segmental dynamics of the polymer. However, with the presence of the lithium salt, the ceramic component slowed the segmental motion of the polymer chains, resulting in a decreased ionic conductivity of the polymer phase in the composite compared to the pure polymer electrolyte.[6] It is clearly very challenging to study the ceramic−polymer composite electrolyte system due to its complexity and the fact that all the components seemingly play a key role in its resulting Li-ion conduction properties, with the latter possibly being further influenced by surface impurities and the incidental formation of additional interphases.[7−9] Nevertheless, the influence of the polymer properties on the Li-ion conductivity of the composite electrolytes has not yet been studied.

$Li_{1+x}Al_xTi_{2-x}(PO_4)_3$ (LATP) is a NASICON-type inorganic solid-state electrolyte with a rather high ionic conductivity of $\sigma \approx 10^{-4}$ S cm^{-1} at 25 °C. The stability of LATP against air, moisture, and most polymer electrolytes can avoid both the undesired initial presence and possible formation of detrimental impurity phases (e.g., Li carbonate) that can occur at the polymer−ceramic interface, as otherwise seen for analogous $Li_7La_3Zr_2O_{12}$ (LLZO) composites.[10−12] These beneficial properties make LATP an excellent material to study the effects and role of the different polymer features on the total ionic conductivity of polymer-in-ceramic composite electrolytes in more detail without incurring such critical interfacial issues.

Previous studies using various ceramic−polymer composite approaches[13−15] have also focused on mitigating the main issue of LATP due its electrochemical instability vs metallic lithium, which causes the reduction of Ti^{4+}, giving rise to a reactive mixed conducting interface that deteriorates LATP and its local contact with lithium, thus leading to a significant increase of interface impedance. Improvements of scarce interface properties of similar NASICON-type solid-state electrolytes were also pursued via composite electrolytes through the use of different polymers and aimed preparation methods.[16,17]

Semicrystalline polyether poly(ethylene oxide) (PEO) has been widely studied for solid polymer electrolyte (SPE) purposes.[18−20] Conversely, polyesters such as poly(ε-caprolactone) (PCL) and poly(ε-caprolactone-*co*-trimethylene carbonate) (P(CL-*co*-TMC)) have recently gained attention for their potential use as alternative host materials for SPEs.[20−23] Polyethers and polyesters have different Li-ion coordinating properties. These polyester-based SPEs have a higher Li-ion mobility relative to the mobility of the counterion compared with PEO SPEs. As such, the PCL and P(CL-*co*-TMC) SPEs are clearly superior in terms of Li-ion transference number with values up to $t_{Li^+} = 0.6$, 3 times higher than that of PEO SPEs ($t_{Li^+} = 0.2$).[24] The high Li-ion transference numbers exhibited by polyester-based SPEs could benefit Li-ion transport through the ceramic−polymer interfaces. Currently, most CPEs are prepared with polymer matrices with low Li-ion transference numbers typically below $t_{Li^+} = 0.2$ and conducting ceramics with very high Li-ion transference numbers ($t_{Li^+} \approx 1$). This mismatch in transference numbers between these two phases could give rise to polarization at the polymer−ceramic interface and is also deemed as one of the causes of high interfacial resistance in this region.[25]

The addition of the minor PTMC comonomer units in P(CL-*co*-TMC) suppresses the crystallization in PCL, while it conveniently maintains similar Li-ion transport properties. This crucial aspect can then constitute a turning point to purposely investigate the effect of such distinctive physical properties, i.e., an amorphous vs semicrystalline polymer matrix, on Li-ion conduction in the CPEs. Furthermore, the PCL and PEO SPEs are both semicrystalline, while their intrinsic Li-ion coordination strengths are clearly different. Therefore, this particular feature can enable an aimed study of the effect of the Li-ion coordination properties on Li-ion conduction in the CPEs, i.e., weak vs strong Li-ion coordination in the polymer matrix. Based on the above considerations, this paper aims to investigate the role of the polymer properties in the Li-ion conductivity of the LATP-PCL:LiTFSI, LATP-P(CL-*co*-TMC):LiTFSI, and LATP-PEO:LiTFSI composite electrolyte systems. Exploring the influence of the polymer matrix on the polymer−ceramic composite electrolytes lays a preliminary foundation to better understand the Li-ion conduction in these composite electrolytes and, accordingly, to design optimized ceramic−polymer electrolytes for advancing all-solid-state batteries.

2. EXPERIMENTAL SECTION

2.1. Preparation of Composite Electrolytes. ε-Caprolactone (CL, Perstorp) was distilled under reduced pressure over CaH_2 (99.9%, Sigma-Aldrich). Trimethylene carbonate (TMC, Richman Chemicals) was used as received and stored in an argon-filled glovebox together with ε-caprolactone. Stannous 2-ethylhexanoate (95%, Sigma-Aldrich) and dry toluene (99.8%, Acros Organics) were also kept in an argon-filled glovebox. The P(CL-*co*-TMC) copolymer (430 kg mol^{-1}) was prepared through bulk ring-opening polymerization, following the same synthesis procedure previously reported.[22] The poly(ethylene oxide) powder (PEO; Sigma-Aldrich, 2×10^6 mol kg^{-1}) and poly(ε-caprolactone) (PCL, Perstorp, 50 kg mol^{-1}) were used as received and stored in an argon-filled glovebox. $Li_{1.4}Al_{0.4}Ti_{1.6}(PO_4)_3$ powder (LATP, >95%, ∼ 1 μm, NEI Corporation) was also used as received and stored in an argon-filled glovebox. Lithium bis(trifluoromethanesulfonyl)imide (LiTFSI, BASF) was dried in a vacuum oven at 120 °C for 48 h.

The composite electrolyte films had embedded 70 wt % (49 vol %) LATP powders, which provided a suitable ceramic amount in the resulting polymer-in-ceramic systems, although the latter could generally require further optimization in terms of ceramic particle content, e.g., depending on the type of particles, particle size, and preparation methods, as these factors ultimately influence the overall electrolyte performance.[26] The composite electrolytes were prepared by first making a viscous polymer−salt mixture by dissolving the polymers and 30 wt % LiTFSI salt in acetonitrile (ACN, Sigma-Aldrich). Then, the LATP particles were added to the mixture, which was subsequently ball-milled at 25 Hz for 15 min under an argon atmosphere. Lastly, the ball-milled mixture was cast in a Teflon mold and vacuum-dried inside the glovebox at 60 °C for 40 h to obtain the composite electrolyte films, following a similar procedure reported in

https://doi.org/10.1021/acsaem.4c00701
ACS Appl. Energy Mater. 2024, 7, 4609−4619

the literature.[27] The resulting composite electrolyte films were further cooled to ambient temperature and subsequently punched to obtain disks with a diameter of 15 mm without leaving the argon atmosphere. Neat polymer electrolytes with the same LiTFSI content were also obtained using a similar method but excluding the ceramic particles. The ceramic−polymer composite electrolyte samples containing the LiTFSI salt were labeled as CPEs, while the composite electrolytes without the LiTFSI salt were labeled as NCPEs. The latter were prepared by employing the same method. High-molecular-weight PEO, PCL, and P(CL-*co*-TMC) polymers were used for the fabrication of their respective composite electrolytes, and this allowed an adequate comparison of the transport dynamics, as at high molecular weights, the polymer segmental dynamics are no longer dependent on the polymer molecular weight.

2.2. Materials Characterization. The crystal structure and purity of the composite electrolytes were studied using X-ray diffraction (XRD) in a 2θ range of 10−40° via a Bruker D8 Advance diffractometer equipped with a Cu Kα radiation source (λ = 1.54178 Å), operating in a Bragg−Brentano geometry.

Fourier transform infrared (FT-IR) spectroscopy analyses were performed at room temperature using a PerkinElmer (Spectrum One) FT-IR spectrometer equipped with a KBr/PE beam splitter, a DTGS/KBr detector, and a Pike GladiATR diamond attenuated total reflectance (ATR) unit and with a resolution of 2 cm^{-1}. The FT-IR measurements were executed in an ATR configuration with spectral acquisitions in the wavenumber range of 4000−530 cm^{-1}.

A Raman spectrometer (Renishaw, inVia) with a built-in optical microscope (Leica) was utilized for the measurements of the ceramic and composite samples. An excitation wavelength of 532 nm produced by a solid-state laser (Renishaw, max power of 500 mW) was employed to acquire the Raman spectra. Prior to the analyses, a calibration of the spectrometer was run via a Si wafer to make sure that a characteristic Raman peak was revealed at around 520 cm^{-1}. The samples were placed onto a glass slide, and a 50× lens was utilized to focus the laser beam onto the surface of the specimens. A constant limited laser power of 0.1% of its maximum nominal value was employed during the analyses to prevent possible detrimental effects on the surface. Spectrum acquisition relied on a measuring time of 20 s and 20 cumulative repetitions to improve the signal-to-noise ratio of the corresponding spectral signals. Minimal sample exposure to the laser beam during subsequent acquisitions was also applied to prevent possible surface degradation.

X-ray photoelectron spectroscopy (XPS) analyses were carried out using a KRATOS Axis Supra+ spectrometer using monochromatic Al Kα radiation (1487 eV) and a dedicated charge neutralizer. All samples were introduced into the spectrometer via a transfer procedure under an inert atmosphere. An airtight sample holder was prepared in an argon-filled glovebox and then opened in the high vacuum chambers in the spectrometer. The spectra, which were acquired with an energy resolution of 0.1 eV/step, were analyzed by means of the CasaXPS software. The spectra for all samples were calibrated in energy using the carbon 1s peak at 284.8 eV. Analysis and fitting of the spectra were carried out using a Shirley and Tougaard background and Gaussian−Lorentzian (30% Lorentzian contribution) line shapes.

Differential scanning calorimetry (DSC) measurements were run using a TA Instruments Q2000 apparatus in the temperature range spanning from −80 to 100 °C (cool/heat/cool/heat) with a heating rate of 10 °C min^{-1} and a cooling rate of 5 °C min^{-1}.

Scanning electron microscopy (SEM) was performed to image the surface morphology of the samples. An SEM microscope (Zeiss, LEO 1550) with a field-emission electron source was used to acquire the topographic images of the various samples at different magnifications via a dedicated In-Lens detector for secondary electrons. Prior to specimen introduction to the SEM vacuum chamber, the composite electrolyte samples were sputtered with an ultrathin, electronically conductive Au/Pd film to enable their surface imaging and thus avoid excessive charging while taking the SEM images. The SEM images were acquired using a low acceleration voltage of 2 kV in order to preserve the features of these sensitive composite samples as much as possible and minimize possible detrimental effects due to their interaction with the electron beam.

2.3. Electrochemical Characterization. The Li-ion conductivity of the composite electrolytes, polymer electrolytes, and ceramic electrolyte were respectively determined by electrochemical impedance spectroscopy (EIS, SI 1260 Impedance Gain-Phase Analyzer, Schlumberger). The electrolyte films were sandwiched between two stainless steel blocking electrodes in a coin-type cell. The cells were heated to 90 °C for 1 h and then cooled to room temperature overnight to improve the contact of the electrolytes with the blocking electrodes. The impedance was measured in the frequency range of 100 mHz−7 MHz using a sinusoidal amplitude of 10 mV in the temperature range of 30−90 °C. The ionic conductivity, σ, was calculated from the relation $\sigma = t/(RA)$, in which t represents the thickness, R the bulk resistance, and A the cross-sectional geometrical area of the electrolyte in contact with the blocking electrodes.

EIS measurements were also carried out for the determination of the resistance between the ceramic and polymer electrolytes. A polymer electrolyte disk was sandwiched between two ceramic disks in a Swagelok-type cell with copper blocking electrodes. The pellets were sputtered with Au/Pd on one side to improve the electrical contact with the copper blocking electrodes. The cells were also heated to 90 °C for 1 h and cooled to room temperature overnight before the measurements, following a protocol analogous to that described above. The impedance measurements were recorded in the frequency range of 100 mHz−7 MHz with an amplitude of 50 mV in the temperature range of 30−90 °C, with the cells equilibrated for 2 h at each temperature before the corresponding EIS spectra were acquired. SPE and CPE films had a typical thickness of ca. 110 μm, and the LATP densified pellet had a thickness of ca. 1100 μm.

The lithium-ion transference number (t_{Li^+}) measurements were performed through a potentiostat (BioLogic SP-240) following the Bruce and Vincent method utilizing a symmetric Li/electrolyte/Li cell configuration in vacuum-sealed pouches. The cells were equilibrated at 60 °C overnight before the measurements. The AC impedance signal was measured between 100 mHz and 7 MHz before and after polarization. A DC polarization voltage of 10 mV was applied. The lithium-ion transference number of the samples was then calculated using the following relationship:

$$t_{Li^+} = \frac{I_{SS}(V - I_0R_0)}{I_0(V - I_{SS}R_{SS})} \quad (1)$$

where I_0 is the initial current, I_{ss} is the steady-state current, R_0 is the initial resistance obtained before polarization, R_{ss} is the steady-state resistance obtained after polarization, and V is the applied polarization voltage. The values of R_0 and R_{ss} were determined by fitting the Nyquist plots to an equivalent circuit (Figure S5) using the BioLogic EC-LAB software. I_0 was calculated using the ratio between the polarization potential and the total resistance across the cell (R_b + R_{int}).

2.4. Solid-State NMR Characterization. Solid-state nuclear magnetic resonance (ssNMR) spectra were recorded at 11.7 T by using a Bruker AVANCE III HD spectrometer. A 3.2 mm cross-polarization magic angle spinning (CP/MAS) probe was used for the ^{1}H, ^{7}Li, and ^{19}F NMR experiments recorded at Larmor frequencies of $\nu(^1H)$ = 500.130 MHz, $\nu(^7Li)$ = 194.317 MHz, and $\nu(^{19}F)$ = 470.59 MHz, respectively. The ^{1}H, ^{7}Li, and ^{19}F chemical shifts were calibrated using adamantane (^{1}H: 1.85 ppm), a 1 M solution of LiCl in D_2O (^{7}Li: 0.0 ppm), and polytetrafluorethylene (^{19}F: −122.0 ppm), respectively, as external standards. Additional details on the ^{13}C NMR results can be found in the Supporting Information. All experiments were carried out at a sample rotation frequency of 20 kHz. In order to gain insight into the dynamics of the investigated systems, NMR measurements were performed at two different temperatures, namely 10 and 30 °C.

A series of ^{7}Li MAS and CP/MAS NMR experiments with various experimental setups was performed. The ^{7}Li MAS NMR measurements were carried out using the application of a 2.5 μs 90° pulse with four scans and various recycle delay times (2, 5, 10, and 20 s). The ^{7}Li

https://doi.org/10.1021/acsaem.4c00701
ACS Appl. Energy Mater. 2024, 7, 4609−4619

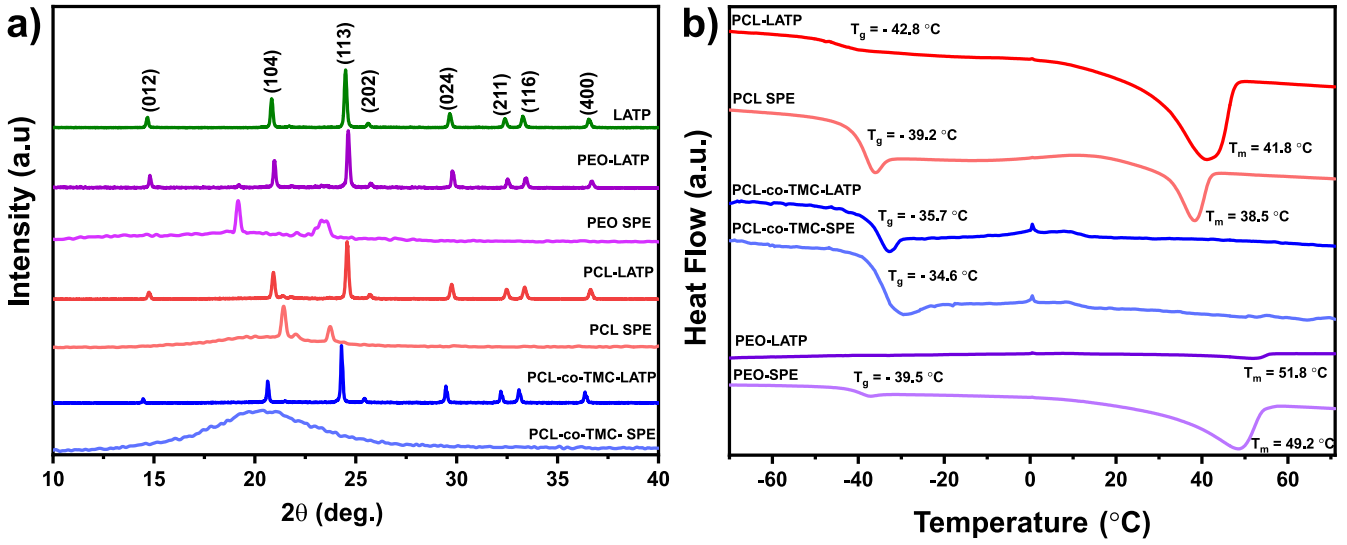

Figure 1. (a) XRD patterns (from top to bottom) of LATP ceramic powder, PEO-LATP CPE, PEO SPE, PCL-LATP CPE, PCL SPE, P(CL-*co*-TMC)-LATP CPE, and P(CL-*co*-TMC) SPE samples. (b) DSC analyses of various electrolyte samples for the PCL, P(CL-*co*-TMC), and PEO SPEs and their respective PCL-LATP, P(CL-*co*-TMC)-LATP, and PEO-LATP CPEs.

CP/MAS NMR experiments were conducted using a 90° pulse with a length of 2.5 μs, a recycle delay of 2 s, four scans, and various CP contact times (100, 1000, 1800, and 5000 μs). An attempt to observe the exchange of Li^+ ions between Li-containing species was made using 2D $^7Li-^7Li$ exchange spectroscopy (EXSY). 2D $^7Li-^7Li$ EXSY correlation MAS NMR spectra were recorded by using a NOESY-type three-pulse sequence. The 90° pulse length was set to 3.0 μs at 60 W. The duration of the spin-exchange periods between the second and third pulse ranged from 100 μs to 500 ms. For all EXSY NMR experiments, the spectral width in the F1 frequency dimension was 20 kHz, and that in the F2 frequency dimension was 50 kHz. The indirect detection period, t_1, consisted of 512 increments, each composed of four scans.

^{19}F MAS experiments were carried out at various temperatures (10 and 30 °C). A 90° pulse with a length of 2.65 μs was used with a 3 s recycle delay and 128 scans. In order to obtain further insights into the dynamics of the investigated systems, ^1H, ^7Li, and ^{19}F T_1 relaxation times were measured using a saturation recovery pulse sequence to follow the mobility of the polymer matrix, Li^+ cations, and $TFSI^-$ anions, respectively. The ^7Li T_1 relaxation times were measured by the application of a 2.5 μs 90° pulse with eight scans and an increasing recycle delay (0.001−12 s) with 10 increments. The ^1H T_1 relaxation times, in turn, were measured using a 2.6 μs 90° pulse with four scans and recycle delays ranging from 0.001 to 4 s with 12 increments. Lastly, the ^{19}F T_1 relaxation experiments were performed using a 2.65 μs 90° pulse with 32 scans and an increasing recycle delay (0.001−12 s) with 12 increments.

All of the samples were packed into ZrO_2 rotors in an argon-filled glovebox. The Bruker TopSpin 3.2 pl5 software package was used for the processing of the spectra, and Bruker Dynamics Center 2.6.1 was used for the analyses of the NMR relaxation data.

3. RESULTS AND DISCUSSION

3.1. Structural and Morphological Characterization.

Figure 1a presents the XRD patterns of the LATP powder, PCL-LATP CPE, P(CL-*co*-TMC)-LATP CPE, PEO-LATP CPE, PCL SPE, PEO SPE, and P(CL-*co*-TMC) SPE samples. The diffraction pattern of the LATP powder was indexed to a standard NASICON-type structure $LiTi_2(PO_4)_3$ with a characteristic space group of *R*3*c* (JCPDS card #35-0754). The strong peaks observed in all of the diffractograms of the various composites correlate with the characteristic reflections of the LATP diffraction pattern. The PCL-LATP CPE shows additional distinctive peaks at 21.39° and 23.72°, arising from the long-range ordered structure of the PCL polymer.[28] The PEO-LATP CPE also exhibits additional peaks at 19.14° and 23.42°, which are related to the ordered structure of the PEO polymer.[29,30] A broad band at around 21° is observed in the diffraction pattern of the P(CL-*co*-TMC) SPE sample due to its amorphous nature. No apparent changes in the reflections associated with the LATP structure or additional diffraction peaks due to the possible decomposition of crystalline products of the constituents in the corresponding composite electrolytes are observed for any of the CPE samples. Although the significant loading of LATP particles is expected to influence the polymer long-range order of PEO and PCL, faint peaks for their characteristic diffractions are still visible in the XRD patterns of their respective composites, thus suggesting that they mostly retained their semicrystalline features, likely due to a moderate degree of mutual dispersion of the polymer and ceramic phases.

The polymer properties within the composite electrolytes were investigated by using FT-IR and DSC analyses. Figure 1b shows the DSC curves of the PEO-LATP, PCL-LATP, and P(CL-*co*-TMC)-LATP CPEs, which are compared to those of their related SPEs. A first DSC scan was applied to erase the thermal history of the samples, while a second scan was used to determine the thermal properties. The P(CL-*co*-TMC) polymer matrix remains amorphous in the P(CL-*co*-TMC)-LATP CPE with a slightly decreased glass transition temperature (T_g) compared to that of the P(CL-*co*-TMC) SPE. The T_g for the P(CL-*co*-TMC) SPE and CPE samples is −34.6 and −35.7 °C, respectively. However, the T_g values decreased for the PCL-LATP and PEO-LATP CPEs compared to their SPE counterparts; in fact, in the PEO-LATP CPE, the T_g disappeared. The PCL SPE and PCL-LATP CPE showed respective T_g values of −39.2 and −42.8 °C and melting temperatures (T_m) of 38.5 and 41.8 °C, respectively. The PEO SPE and PEO-LATP CPE exhibited T_m values of 49.5 and 51.8 °C, respectively. The T_g of the PEO SPE is −39.5 °C. The reduction of the T_g values indicates that the polymer matrix in the CPEs has polymer (thermal) properties that are different from those originally found in the polymer matrix in the SPEs.

https://doi.org/10.1021/acsaem.4c00701
ACS Appl. Energy Mater. 2024, 7, 4609−4619

This could be due to the occurrence in which the bulk polymer could be transformed into an interfacial polymer layer at this high ceramic loading within the CPEs or at least exhibit properties similar to a bound polymeric layer. An adsorbed "bound" polymer layer near the surface of ceramic particles in polymer−ceramic composite systems has been reported previously.[31,32] This bound polymer layer was found to have properties different to those of the bulk polymer.[31−33] An interfacial layer is said to form near the surface of ceramic particles at very high ceramic loadings with properties different from the polymer bulk.[4,5] Additionally, according to Qiao et al., this decrease in T_g observed for the polymer−ceramic composites is also correlated to an increase in particle agglomeration due to self-attraction of the particles and high surface tension during materials processing.[34] Indeed, the SEM analysis (Figure 2) revealed LATP particle agglomeration in the CPEs.

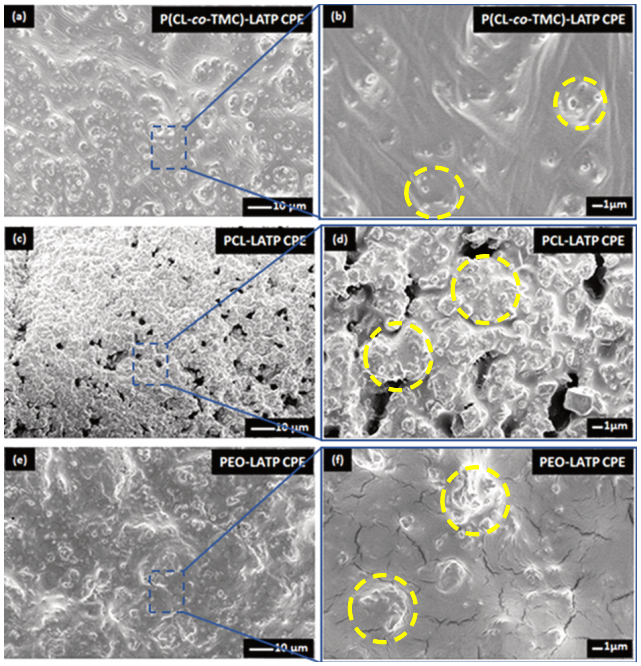

Figure 2. SEM images at different magnifications of (a, b) P(CL-*co*-TMC)-LATP CPE, (c, d) PCL-LATP CPE, and (e, f) PEO-LATP CPE samples. The scale bars in the micrographs are 10 μm (left) and 1 μm (right). The yellow dashed circles in the images at higher magnification highlight the morphological features of the LATP particles and their embedded agglomerates in the respective surrounding polymer matrices.

The slight increase in the T_m values only indicates the different thermomechanical properties of the polymer in the CPEs compared to the SPE bulk. The structure of the polymer matrix in the composite electrolytes is similar to that of the SPE counterparts, as confirmed by ^{13}C NMR and FT-IR analyses, shown separately in Figure S1.

Figure 2a−f displays a series of SEM images respectively taken for the (a, b) P(CL-*co*-TMC)-LATP CPE, (c, d) PCL-LATP CPE, and (e, f) PEO-LATP CPE samples under different magnification conditions. The SEM images show the distribution of the LATP particles in their respective polymer matrices. Although the particles were covered by the polymer matrix in each CPE, the particles appeared agglomerated, and gaps (i.e., pores) were also observed among the particles. This can represent an obstacle to Li-ion conduction, unless aimed preheating of the composites in corresponding electrode/electrolyte stacks is performed prior to their electrochemical characterization in order to address such a potential issue. The cracks observed in Figure 2f were most likely due to the exposure of the sample to the electron beam during image acquisition.

3.2. Ion Dynamics in Composite Electrolytes. Solid-state NMR measurements were performed at two temperatures (10 and 30 °C) to determine the dynamics in the CPEs. It is crucial to investigate the effect of LATP particle agglomeration on the ion (cation and anion) and polymer chain dynamics of the different SPE matrices, as this clearly impacts the overall response of the corresponding CPEs. The ^{1}H, ^{7}Li, and ^{19}F T_1 relaxation experiments provided valuable information about the dynamics in the composite electrolytes. Table 1 reports the measured ^{1}H, ^{7}Li, and ^{19}F T_1 relaxation times corresponding to the dynamics of the polymer matrices, Li^+ cations, and $TFSI^-$ anions. ^{1}H T_1 relaxation measurements reveal that the relaxation times of the polymer matrix in the investigated samples decrease with increasing temperature, meaning that the matrix is immobilized and is in the slow-motion regime.[35]

This could explain the changes in the thermomechanical properties of the composite electrolyte polymer matrix, as previously observed in the DSC analyses. The measured T_1 (^{1}H) times (Table 1) clearly show that the PEO matrix possesses slower network dynamics at 10 °C in comparison with the other investigated matrices, as its relaxation time is higher than those for PCL and P(CL-*co*-TMC). This is not surprising, as at this temperature, PEO is typically semicrystalline, whereas at least P(CL-*co*-TMC) is amorphous. A steep decrease in relaxation time from 0.91 to 0.54 s is observed for the PEO composite system, which demonstrates considerable energetic barriers to the polymer segmental motion in the PEO matrix compared to those of the PCL and P(CL-*co*-TMC) copolymer. The PCL chains, in turn, are slightly less mobile

Table 1. Experimentally Measured ^{1}H, ^{7}Li, and ^{19}F T_1 Relaxation Times Corresponding to Dynamics of the Polymer Matrices, Li^+ Cations, and $TFSI^-$ Anions

			T_1 (^{7}Li) (s)		
sample	temperature (K)	T_1 (^{1}H) (s)	Li (polymer)	Li (LATP)	T_1 (^{19}F) (s)
LATP-PEO:LiTFSI	283	0.91 ± 0.04	0.12 ± 0.07	0.05 ± 0.02	0.59 ± 0.02
	303	0.54 ± 0.03	0.09 ± 0.05	0.02 ± 0.01	0.66 ± 0.08
LATP-PCL:LiTFSI	283	0.68 ± 0.07	0.70 ± 0.3	0.04 ± 0.02	0.47 ± 0.01
	303	0.53 ± 0.02	0.40 ± 0.2	0.02 ± 0.01	0.57 ± 0.01
LATP-P(CL-*co*-TMC):LiTFSI	283	0.59 ± 0.05	0.50 ± 0.2	0.04 ± 0.02	0.47 ± 0.01
	303	0.54 ± 0.02	0.40 ± 0.2	0.02 ± 0.01	0.54 ± 0.01

https://doi.org/10.1021/acsaem.4c00701
ACS Appl. Energy Mater. 2024, 7, 4609−4619

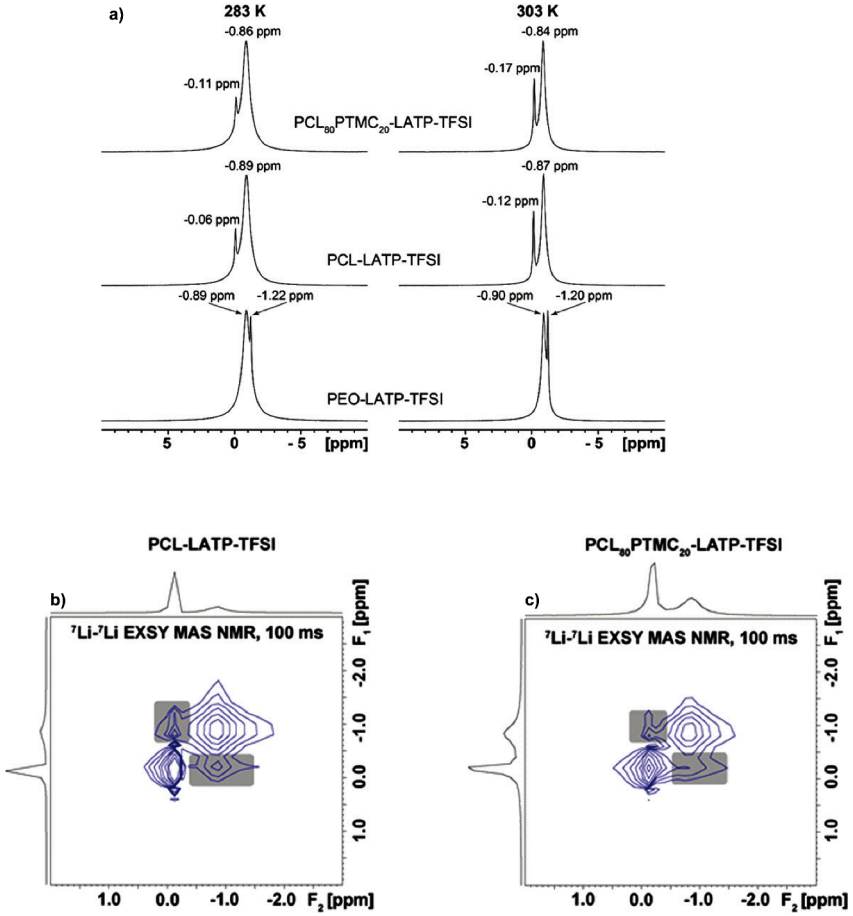

Figure 3. (a) ^{7}Li MAS NMR spectra of LATP-PEO:LiTFSI, LATP-PCL:LiTFSI, and LATP-P(CL-*co*-TMC):LiTFSI samples measured at 10 °C (left column) and 30 °C (right column). (b, c) 2D ^{7}Li−^{7}Li EXSY spectra recorded under MAS (20 kHz) at 30 °C for the (b) LATP-PCL:LiTFSI composite electrolyte and (c) LATP-P(CL-*co*-TMC):LiTFSI sample at a mixing time of 100 ms.

than those of the P(CL-*co*-TMC) copolymer, based on the obtained T_1 (^{1}H) times of 0.68 and 0.59 s at 10 °C, respectively.

Figure 3a shows the ^{7}Li MAS NMR spectra of the LATP-PCL:LiTFSI, LATP-PEO:LiTFSI, and LATP-P(CL-*co*-TMC):LiTFSI samples measured at 283 (left column) and 303 K (right column). The ^{7}Li T_1 relaxation time measurements allowed for distinguishing the mobility of the Li^{+} ions in the polymer and the ceramic phase (LATP).

In general, the relaxation time of Li^{+} in both environments decreases with increasing temperature, thus indicating that its mobility falls in the slow-motion regime, as was observed for the investigated polymer matrices. The dynamics of the Li^{+} cations in LATP are not influenced by the polymer matrix, as it exhibits almost the same values of T_1 times in all three samples (Table 1). However, the mobility of Li^{+} inside a polymer matrix is different for the different samples. It should be noted that some uncertainty in the determination of the ^{7}Li T_1 relaxation times in the polymer may arise because of an overlapping of the broad peak from LATP with the narrow peak from the polymer (Figure 3a). Figure S2 shows the ^{19}F MAS NMR spectra of the LATP-PCL:LiTFSI, LATP-PEO:LiTFSI, and LATP-P(CL-*co*-TMC):LiTFSI samples measured at 10 (left column) and 30 °C (right column). It is evident from the measurements of the ^{19}F T_1 times, corresponding to the TFSI^{-} anion, that the PEO sample possesses higher values of ^{19}F T_1 and, therefore, slower anion dynamics than its PCL and P(CL-*co*-TMC) counterparts. The rate of the anion dynamics in PCL and P(CL-*co*-TMC), in turn, is almost identical, as the respective T_1 values are similar (Table 1).

To achieve the high ionic conductivity in the composite electrolytes promised by the ideal picture of combining the ceramic electrolyte with the polymer electrolyte, it has become clear that facile transport of Li^{+} ions "across" the polymer and ceramic interface should be achieved. Thus, homonuclear 2D ^{7}Li−^{7}Li EXSY NMR spectroscopy was applied to gain insights into the Li-ion transport between the polymer and LATP phases in the composite electrolytes. The experiments were performed at two different temperatures (10 and 30 °C) with various mixing times (from 100 μs to 500 ms), allowing for monitoring of the Li−Li exchange at different rates. Figure 3b,c shows the 2D ^{7}Li−^{7}Li EXSY spectra recorded under MAS (20 kHz) at 30 °C for the LATP-PCL:LiTFSI and LATP-P(CL-*co*-TMC):LiTFSI samples. Surprisingly, the exchange was not detected in the case of the composite with PEO, as no cross-peaks were detected in the corresponding spectra, suggesting that the exchange is either absent or too slow to observe. This is probably due to the strong affinity of the Li^{+} ions toward the PEO matrix, which effectively suppresses or even hampers the transporting of Li^{+} ions over the phase boundary. Quantitative analysis of the evolution of cross-peak intensity is highly uncertain due to the very short T_1 (^{7}Li) relaxation times, which are even shorter than the applied mixing times. Probably due

https://doi.org/10.1021/acsaem.4c00701
ACS Appl. Energy Mater. 2024, 7, 4609−4619

to this fast relaxation, the correlation signals disappear at long mixing times (250 ms), as observed for the LATP-P(CL-*co*-TMC):LiTFSI sample. Perhaps this phenomenon can also be responsible for the absence of correlation signals in the 2D ^{7}Li−^{7}Li EXSY NMR spectra of the PEO-based systems recorded at long mixing times. However, even with this explanation, the PEO:LATP interfacial exchange of Li^+ ions seems to be of low rate and efficiency because the correlation signals are not detectable also at short mixing times. In contrast, for the systems with PCL and P(CL-*co*-TMC) polymer matrices, particularly at high temperature, the cross-peaks revealing the exchange of Li^+ between the polymer and ceramic phases were clearly detected in the 2D ^{7}Li−^{7}Li EXSY NMR spectra (Figure 3b,c). At low temperature (10 °C), for which the ion transport in the polymer phase is significantly more sluggish, however, even these cross-peaks disappear and are absent, which indicates that decreasing the temperature switches off the interfacial transfer of Li^+ ions, when they preferentially stay separated in the polymer and ceramic phases.

These results indicate that in the PEO matrix, compared to the PCL and P(CL-*co*-TMC) matrices, the transport of the Li^+ cations between the polymer phase and the ceramic phase is still very slow or nonexistent. This difference in the interfacial transport of Li^+ ions across the polymer−ceramic interface between the PEO and the polyester polymers PCL and P(CL-*co*-TMC) could be mainly attributed to the difference in Li−polymer coordination strengths between the polyether polymers and the polyester polymers.

3.3. Ionic Conductivity Measurements. The effect of different polymer−Li ion coordinations on the lithium transport was investigated by measuring the Li-ion conductivity of the samples. Since no interphase products were observed from the previous XRD and spectroscopic analyses, the Li-ion transport in the CPEs is not expected to be hindered by any additional (e.g., Li^+ blocking) interface contributing to impedance and, thus, should only include the transport involving the polymer matrix and the LATP ceramic. Figure 4a−c shows the temperature dependence of the total ionic conductivity of the PCL, P(CL-*co*-TMC), and PEO composite electrolytes with dissolved LiTFSI salt (CPEs), without the LiTFSI salt (NCPEs), SPEs, and LATP pellet, respectively.

All of the studied CPEs exhibit a lower ionic conductivity compared to their SPEs and the densified LATP pellet. The total ionic conductivities of the ceramic electrolyte, polymer electrolytes, and composite electrolytes are shown in Table S1. Hence, the low ionic conductivity in the composite electrolytes would most likely be attributed to agglomeration of the ceramic particles within the CPEs. This, in turn, would possibly provoke the disappearance of a ceramic percolation network and the disruption of the ceramic ion-conducting pathways with a concurrent disruption of the continuity of Li-ion transport pathways in the polymer matrix caused by the high loading of the ceramic particles. These results suggest that the effect of particle agglomeration can most likely dominate the benefits of a good polymer matrix in a composite electrolyte, especially when high ceramic loadings are purposely included to achieve polymer-in-ceramic electrolyte systems. Under such conditions, the tendency toward particle agglomeration can only increase with increasing mass fractions for the ceramic component. As long as there exists agglomeration in the composite electrolytes, the comparatively fast transport across the polymer−ceramic interface promised by the polyester-based PCL and P(CL-*co*-TMC) composites, compared to that of their PEO analogue, will not bring a benefit in the total conductivity of these composite electrolytes. Additionally, as determined by solid-state NMR analysis, the dynamics of the Li^+ ions and polymer chains within the CPEs were found to be in the slow-motion regime (see Figure S3), irrespective of the polymer matrix used.

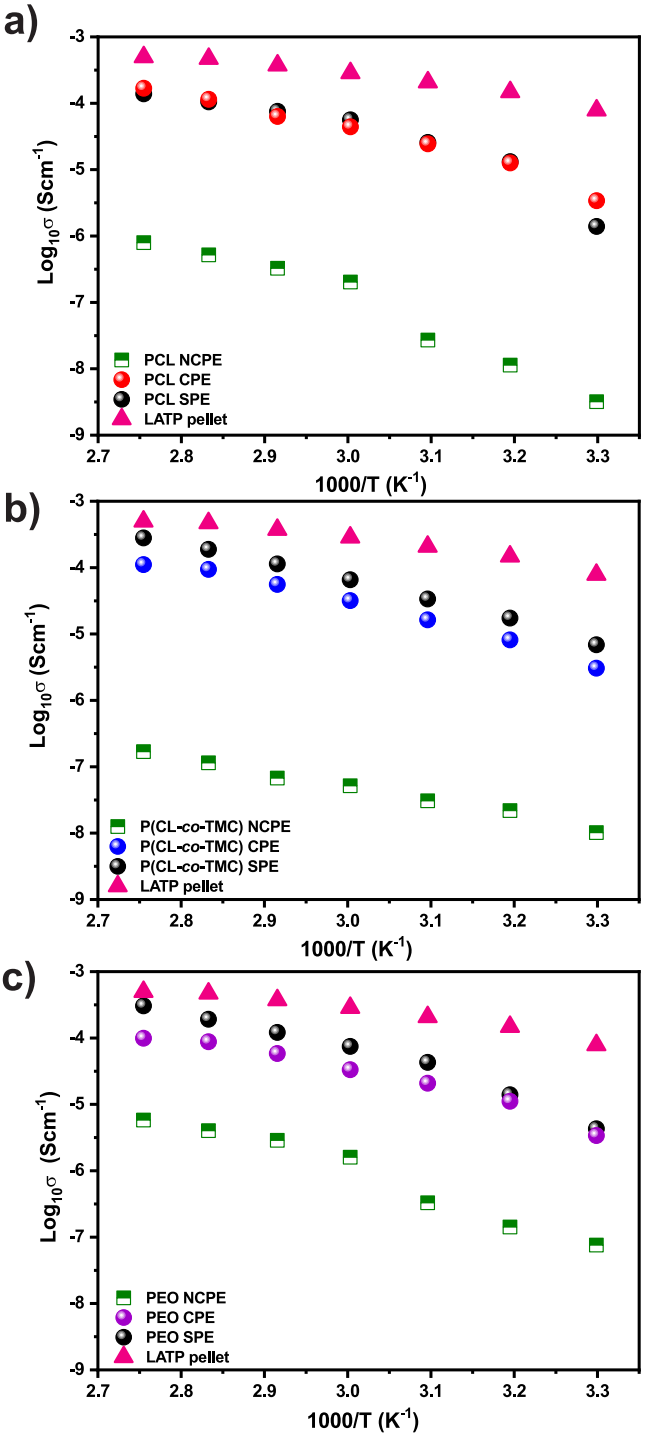

Figure 4. Ionic conductivity measurements of (a) PCL-NCPE, PCL-CPE, PCL-SPE, and LATP pellet, (b) P(CL-*co*-TMC) NCPE, P(CL-*co*-TMC) CPE, P(CL-*co*-TMC) SPE, and LATP pellet, and (c) PEO-NCPE, PEO−CPE, PEO-SPE, and LATP pellet.

https://doi.org/10.1021/acsaem.4c00701
ACS Appl. Energy Mater. 2024, 7, 4609−4619

In the absence of the LiTFSI salt, the NCPEs display low ionic conductivity compared to their CPE and SPE counterparts. This can be rationalized based on the following: (i) the severe lack of free mobile Li^+ ions and (ii) the scarce wettability of the ceramic by the polymer without salt, thus unavoidably decreasing the rate of transport of the Li^+ ions between these two phases. In any case, this hints that in the CPEs, the Li-ion transport through the polymer matrix plays a key role and becomes a limiting factor in the absence of a percolating network for the ceramic particles, thus ultimately affecting the total Li-ion conductivity of the composite electrolytes. Figure S4 compares the impedance of CPEs and NCPEs for the PCL-LATP, P(CL-*co*-TMC)-LATP, and PEO-LATP samples and shows a drastically reduced impedance for these CPEs with respect to the NCPEs.

3.4. Li-Ion Transference Number Characterization. Li-ion transference number measurements (Figure S5) were performed to assess the Li-ion transport properties in the composite electrolytes. The LATP is a single-ion conductor and is expected to have a Li-ion transference number of unity, ideally. The Li-ion transference number of the PEO-LATP, PCL-LATP, and P(CL-*co*-TMC)-LATP CPEs was measured at 60 °C to rule out the limiting effect of the polymer crystallinity in the composite electrolytes. The Li-ion transference number in the composite electrolytes was 0.84, 0.85, and 0.39 for the PCL-LATP, P(CL-*co*-TMC)-LATP and PEO-LATP CPEs, respectively, following the trend in the Li-ion transference number observed from their SPE counterparts. Conversely, the lithium transference number was 0.49, 0.60, and 0.16 for the PCL, P(CL-*co*-TMC), and PEO SPEs, respectively. Accordingly, the Li-ion transference number in all samples is increased by the addition of the LATP particles. Note that the P(CL-*co*-TMC) SPE has a higher transference number compared to the PCL SPE because of the presence of carbonate groups, which results in an overall weaker binding between the coordinating carbonyl groups and the Li^+ ions.[13,34] The weaker coordination in the carbonyl-coordinating polyester SPEs, such as PCL and P(CL-*co*-TMC), leads to less immobilization of the Li^+ ions, thus resulting in higher lithium transference numbers.[36] Vice versa, the strong Li-ion coordination in the polyether host results in a low mobility of the Li^+ ions, making the anions responsible for the majority of the charge transport; thus, there is a lower transference number in the PEO SPE. Indeed, the ^{19}F MAS NMR data confirmed the slower $TFSI^-$ anion dynamics in the PEO-LATP CPE compared to those in the PCL-LATP and P(CL-*co*-TMC)-LATP CPEs.

The Li-ion transference number is still higher in the PCL-LATP and P(CL-*co*-TMC)-LATP CPEs compared to the PEO-LATP CPE. This consideration is important because it confirms in a way that the main limiting factor is still the polymer and its conducting properties. If the transport was dominated by the ceramic particles (and thus t_{Li^+} possibly rather close to 1), the presence of one polymer electrolyte or another would not make such a noticeable difference, especially if ultimately the polymers are practically molten at 60 °C. These Li-ion transference number results indicate the possibility of having more Li^+ ions to transport in these composite electrolyte systems. However, agglomeration in all the samples and resistive polymer−ceramic interfaces, as in the case of the PEO-LATP sample, limit the total ionic conductivity of the composite electrolyte samples.

On the other hand, the beneficial effect that the LATP particles can have on the $TFSI^-$ anion immobilization and their impact on the Li-ion transference number are important aspects that need to be clarified. The preliminary XPS and Raman results obtained here can suggest, although not conclusively, that $TFSI^-$ anion immobilization by LATP may be possible for these composite electrolytes. XPS analyses (Figure S6) were performed for the LATP powder, SPEs, and CPEs, with the latter being particularly challenging to analyze in a consistent way due to their limited interdispersion of the ceramic and polymer phases in proximity of the outermost surface of corresponding samples. The spectra were calibrated with respect to the characteristic C 1s peak of adventitious carbon at 284.8 eV. Figure S6a shows the C 1s spectra of the SPEs, CPEs, and LATP powder. The peaks in the energy range of 284.8−285.1 eV correspond to the aliphatic carbons originating from the polymers and adventitious carbon. The signals obtained at 286.8, 289.1, and 290.7 eV correspond to the ether group (C−O−C) in the PEO polymer, the carbonyl carbon in the ester group (O−C═O) in the PCL polymer, and the carbonate group O−(C═O)−O of the TMC unit in the P(CL-*co*-TMC) copolymer, respectively.[37,38] The peak at around 291−292 eV is attributed to the $-CF_3$ group from the dissolved LiTFSI salt and appears slightly shifted to higher binding energies in the composite electrolytes associated with the PCL-LATP and P(CL-*co*-TMC)-LATP CPEs compared to their SPE counterparts, whereas such a peak shift is actually negligible for the PEO-LATP CPE and PEO SPE. In the F 1s region (Figure S6b), one peak at ∼688.5 eV is observed for all the CPEs and SPEs and is attributed to the $-CF_3$ group in the dissolved LiTFSI salt. This peak is slightly shifted to lower binding energies for all CPEs compared with their SPE counterparts. Likewise, in the N 1s spectra (Figure S6c), the observed peak attributed to the dissolved LiTFSI salt appears also shifted to lower binding energies for all the CPEs compared to their SPEs (see Tables S2 and S3 for further detail on the peak positions). Similarly, Figure S7 shows the Raman spectroscopy measurements of LATP and the PEO-LATP, PCL-LATP, and P(CL-*co*-TMC)-LATP CPEs. The spectra of all the composite electrolyte samples are dominated by the predominant bands arising from the vibrational modes of LATP. The Raman bands centered at around 1100−1300 and 1000 cm^{-1} are attributed to the stretching vibrations of the PO_2 and PO_3 units in LATP, respectively.[39,40] The Raman bands at 450 and ca. 300−350 cm^{-1} are assigned to the symmetrical bending vibrations and motions of the PO_4^{3-} groups, respectively.[39,41] The Raman band at around 273 cm^{-1} is attributed to the translational vibration modes of Ti^{4+} in LATP.[40,41] The bands in the lower wavenumber region between 100 and 250 cm^{-1} are assigned to the transitional vibrations and libration modes of PO_4^{3-} in LATP.[39,41,42] Only very slight changes, if any, are observed for the peaks below 450 cm^{-1} in the Raman bands for the CPEs. Therefore, this analysis alone could not conveniently pinpoint the interaction of the $TFSI^-$ anions with the PO_4^{3-} groups of LATP. Nevertheless, such a type of interaction is legitimately expected here, as interactions among the ceramic particles and the polymer−LiTFSI matrix have previously been reported for composite electrolytes[43−45] having LATP as a ceramic component, among others.

4. CONCLUSIONS

Polymer−ceramic composite electrolytes with high ceramic loading (70 wt % LATP) were prepared using polymer electrolytes (PCL, P(CL-*co*-TMC), and PEO) with different

https://doi.org/10.1021/acsaem.4c00701
ACS Appl. Energy Mater. 2024, 7, 4609−4619

polymer properties. The results of this work highlight a series of important aspects that are crucial in the development of functional CPEs with high loadings of Li-containing ceramic particles (i.e., polymer-in-ceramic composite systems):

(i) The impact of the Li−polymer coordination strength of the polymer matrix on the Li-ion transport in composite electrolytes, especially the one taking place across the polymer−ceramic interface, which is a key feature in order to conveniently bridge the contributions of these two distinctive Li-ion conducting phases. The polyester-based LATP composite electrolytes employing PCL and P(CL-*co*-TMC) with weak Li−polymer coordination strength exhibited a faster exchange of Li^+ ions between the polymer and the ceramic phase compared to the polyether PEO-based LATP composite electrolyte, which had strong Li−polymer coordination strength.

(ii) The effects of particle agglomeration on the total Li-ion conductivity of the composite electrolytes. Agglomeration occurred irrespective of the type of polymer matrix used for the composite electrolytes (i.e., amorphous or semicrystalline, fast Li-ion dynamics or slow Li-ion dynamics). These results remark the necessity to adopt aimed strategies to avoid particle agglomeration in composite electrolytes in order to reach high ionic conductivities; this is especially relevant for polymer-in-ceramic composite systems that heavily rely on high ceramic particle loadings.

(iii) The observation that semicrystalline and amorphous polymer matrices, in the case of PCL- and P(CL-*co*-TMC)-based LATP composite electrolytes, have similar ion (Li^+ and $TFSI^-$) dynamics and transference numbers. This also aligns quite well with the overall picture of these alternative polymeric hosts from earlier investigations.

Therefore, the results obtained in this work are clearly important for understanding in more detail the behavior of this type of polymer-in-ceramic composite electrolytes, and this will aid in selecting suitable polymer matrices for the realization of improved composite electrolytes for applications in all-solid-state batteries.

■ ASSOCIATED CONTENT

Supporting Information

The Supporting Information is available free of charge at https://pubs.acs.org/doi/10.1021/acsaem.4c00701.

^{13}C MAS and CP/MAS NMR spectra, FT-IR analysis, XPS analysis, and Raman spectra of PEO-LATP, PCL-LATP, and P(CL-*co*-TMC)-LATP CPEs; ^{19}F MAS NMR spectra of PEO-LATP-LiTFSI, PCL-LATP-TFSI, and $PCL_{80}PTMC_{20}$-LATP-TFSI samples; schematic representation of T_1 relaxation time vs mobility of investigated species; Li-ion conductivities of the studied ceramic, polymer, and composite electrolytes; impedance of CPEs and NCPEs; and Li-ion transference number measurements (PDF)

■ AUTHOR INFORMATION

Corresponding Author

Mario Valvo − *Department of Chemistry − Ångström Laboratory, Uppsala University, SE-75121 Uppsala, Sweden;* orcid.org/0000-0002-0069-8707; Email: mario.valvo@kemi.uu.se

Authors

Funeka P. Nkosi − *Department of Chemistry − Ångström Laboratory, Uppsala University, SE-75121 Uppsala, Sweden*

Ignacio Cuevas − *Department of Chemistry − Ångström Laboratory, Uppsala University, SE-75121 Uppsala, Sweden*

Jonas Mindemark − *Department of Chemistry − Ångström Laboratory, Uppsala University, SE-75121 Uppsala, Sweden;* orcid.org/0000-0002-9862-7375

Andrii Mahun − *Institute of Macromolecular Chemistry of the Czech Academy of Sciences, 162 06 Prague 6, Czech Republic; Department of Physical and Macromolecular Chemistry, Faculty of Science, Charles University, 8128 40 Prague 2, Czech Republic;* orcid.org/0000-0003-1057-2910

Sabina Abbrent − *Institute of Macromolecular Chemistry of the Czech Academy of Sciences, 162 06 Prague 6, Czech Republic;* orcid.org/0000-0003-4228-4059

Jiří Brus − *Institute of Macromolecular Chemistry of the Czech Academy of Sciences, 162 06 Prague 6, Czech Republic;* orcid.org/0000-0003-2692-612X

Libor Kobera − *Institute of Macromolecular Chemistry of the Czech Academy of Sciences, 162 06 Prague 6, Czech Republic;* orcid.org/0000-0002-8826-948X

Kristina Edström − *Department of Chemistry − Ångström Laboratory, Uppsala University, SE-75121 Uppsala, Sweden;* orcid.org/0000-0003-4440-2952

Complete contact information is available at: https://pubs.acs.org/10.1021/acsaem.4c00701

Notes

The authors declare no competing financial interest.

■ ACKNOWLEDGMENTS

The authors acknowledge the Swedish Energy Agency under Contract 2017-013571, the Swedish Excellence Center Base funded by Vinnova, the Grant Agency of the Czech Republic (Grant GA24-10199S), the Swedish Electromobility Centre (SEC) via Project 12038, and STandUP for Energy for the financial support. Alina Oltean and Fredrik Lindgren are acknowledged for valuable technical support.

■ REFERENCES

(1) Li, S.; Zhang, S.; Shen, L.; Liu, Q.; Ma, J.; Lv, W.; He, Y.; Yang, Q. Progress and Perspective of Ceramic/Polymer Composite Solid Electrolytes for Lithium Batteries. *Advanced Science* **2020**, *7* (5), No. 1903088.

(2) Zhu, X.; Wang, K.; Xu, Y.; Zhang, G.; Li, S.; Li, C.; Zhang, X.; Sun, X.; Ge, X.; Ma, Y. Strategies to Boost Ionic Conductivity and Interface Compatibility of Inorganic - Organic Solid Composite Electrolytes. *Energy Storage Materials* **2021**, *36*, 291−308.

(3) Li, Z.; Huang, H. M.; Zhu, J. K.; Wu, J. F.; Yang, H.; Wei, L.; Guo, X. Ionic Conduction in Composite Polymer Electrolytes: Case of PEO:Ga-LLZO Composites. *ACS Appl. Mater. Interfaces* **2019**, *11* (1), 784−791.

(4) Hanson, B.; Pryamitsyn, V.; Ganesan, V. Mechanisms Underlying Ionic Mobilities in Nanocomposite Polymer Electrolytes. *ACS Macro Lett.* **2013**, *2* (11), 1001−1005.

(5) Mogurampelly, S.; Ganesan, V. Influence of nanoparticle surface chemistry on ion transport in polymer nanocomposite electrolytes. *Solid State Ionics* **2016**, *286*, 57−65.

(6) Chen, X. C.; Sacci, R. L.; Osti, N. C.; Tyagi, M.; Wang, Y.; Palmer, M. J.; Dudney, N. J. Study of segmental dynamics and ion transport in polymer-ceramic composite electrolytes by quasi-elastic

neutron scattering. *Molecular Systems Design and Engineering* **2019**, *4* (2), 379−385.
(7) Cuevas, I.; Nkosi, F.; Edström, K.; Valvo, M. $Li_7La_3Zr_2O_{12}$ interface functionalization via boric acid treatment: A step to contact improvement. *Appl. Surf. Sci.* **2024**, *656*, No. 159611.
(8) Stegmaier, S.; Schierholz, R.; Povstugar, I.; Barthel, J.; Rittmeyer, S. P.; Yu, S.; Wengert, S.; Rostami, S.; Kungl, H.; Reuter, K.; Eichel, R. A.; Scheurer, C. Nano-Scale Complexions Facilitate Li Dendrite-Free Operation in LATP Solid-State Electrolyte. *Adv. Energy Mater.* **2021**, *11* (26), 2100707 DOI: 10.1002/aenm.202100707.
(9) Liu, J.; Liu, T.; Pu, Y.; Guan, M.; Tang, Z.; Ding, F.; Xu, Z.; Li, Y. Facile synthesis of NASICON-type $Li_{1.3}Al_{0.3}Ti_{1.7}(PO_4)_3$ solid electrolyte and its application for enhanced cyclic performance in lithium ion batteries through the introduction of an artificial Li3PO4 SEI layer. *RSC Adv.* **2017**, *7* (74), 46545−46552.
(10) Huo, H.; Li, X.; Sun, Y.; Lin, X.; Doyle-Davis, K.; Liang, J.; Gao, X.; Li, R.; Huang, H.; Guo, X.; Sun, X. Li_2CO_3 effects: New insights into polymer/garnet electrolytes for dendrite-free solid lithium batteries. *Nano Energy* **2020**, *73*, 104836.
(11) Guo, Y.; Cheng, J.; Zeng, Z.; Li, Y.; Zhang, H.; Li, D.; Ci, L. Li_2CO_3: Insights into Its Blocking Effect on Li-Ion Transfer in Garnet Composite Electrolytes. *ACS Applied Energy Materials* **2022**, *5* (3), 2853−2861.
(12) Gupta, A.; Sakamoto, J. Controlling ionic transport through the PEO-LITFSi/LLZTO interface. *Electrochemical Society Interface* **2019**, *28* (2), 63−69.
(13) Wang, Q.; Yang, A.; Ma, J.; Yao, M.; Geng, S.; Liu, F. Constructing PTFE@LATP composite solid electrolytes with three-dimensional network for high-performance lithium batteries. *Electrochim. Acta* **2023**, *467*, No. 143138.
(14) Zhu, L.; Wang, Y.; Wu, Y.; Feng, W.; Liu, Z.; Tang, W.; Wang, X.; Xia, Y. Boron Nitride-Based Release Agent Coating Stabilizes $Li_{1.3}Al_{0.3}Ti_{1.7}(PO_4)_3$/Li Interface with Superior Lean-Lithium Electrochemical Performance and Thermal Stability. *Adv. Funct. Mater.* **2022**, *32* (29), 1−11.
(15) Li, Y.; Wang, H. Composite solid electrolytes with NASICON-type LATP and PVdF- HFP for solid-state lithium batteries. *Ind. Eng. Chem. Res.* **2021**, *60* (3), 1494−1500.
(16) Amici, J.; Romanin, S.; Alidoost, M.; Versaci, D.; Francia, C.; Smeacetto, F.; Bodoardo, S. UV-cured methacrylate based polymer composite electrolyte for metallic lithium batteries. *J. Electroanal. Chem.* **2019**, *837*, 103−107.
(17) Das, A.; Goswami, M.; Illath, K.; Ajithkumar, T. G.; Arya, A.; Krishnan, M. Synthesis and characterization of LAGP-glass-ceramics-based composite solid polymer electrolyte for solid-state Li-ion battery application. *J. Non-Cryst. Solids* **2021**, *558*, No. 120654.
(18) Gorecki, W.; Jeannin, M.; Belorizky, E.; Roux, C.; Armand, M. Physical properties of solid polymer electrolyte PEO(LiTFSI) complexes. *J. Phys.: Condens. Matter* **1995**, *7* (34), 6823.
(19) Jiang, Y.; Yan, X.; Ma, Z.; Mei, P.; Xiao, W.; You, Q.; Zhang, Y. Development of the PEO based solid polymer electrolytes for all-solid state lithium ion batteries. *Polymers* **2018**, *10* (11), 1237.
(20) Mindemark, J.; Lacey, M. J.; Bowden, T.; Brandell, D. Beyond PEO—Alternative host materials for Li^+-conducting solid polymer electrolytes. *Prog. Polym. Sci.* **2018**, *81*, 114−143.
(21) Sun, B.; Mindemark, J.; VMorozov, E.; Costa, L. T.; Bergman, M.; Johansson, P.; Fang, Y.; Furó, I.; Brandell, D. Ion transport in polycarbonate based solid polymer electrolytes: Experimental and computational investigations. *Phys. Chem. Chem. Phys.* **2016**, *18* (14), 9504−9513.
(22) Mindemark, J.; Sun, B.; Törmä, E.; Brandell, D. High-performance solid polymer electrolytes for lithium batteries operational at ambient temperature. *J. Power Sources* **2015**, *298*, 166−170.
(23) Fonseca, C. P.; Rosa, D. S.; Gaboardi, F.; Neves, S. Development of a biodegradable polymer electrolyte for rechargeable batteries. *J. Power Sources* **2006**, *155* (2), 381−384.
(24) Eriksson, T.; Mace, A.; Mindemark, J.; Brandell, D. The role of coordination strength in solid polymer electrolytes: Compositional dependence of transference numbers in the poly(ϵ-caprolactone)-poly(trimethylene carbonate) system. *Phys. Chem. Chem. Phys.* **2021**, *23* (45), 25550−25557.
(25) Merrill, L. C.; Chen, X. C.; Zhang, Y.; Ford, H. O.; Lou, K.; Zhang, Y.; Yang, G.; Wang, Y.; Wang, Y.; Schaefer, J. L.; Dudney, N. J. Polymer-Ceramic Composite Electrolytes for Lithium Batteries: A Comparison between the Single-Ion-Conducting Polymer Matrix and Its Counterpart. *ACS Applied Energy Materials* **2020**, *3* (9), 8871−8881.
(26) Amici, J.; Calderón, C. A.; Versaci, D.; Luque, G.; Barraco, D.; Leiva, E.; Francia, C.; Bodoardo, S. Composite polymer electrolyte with high inorganic additive contents to enable metallic lithium anode. *Electrochim. Acta* **2022**, *404*, No. 139772.
(27) Nkosi, F. P.; Valvo, M.; Mindemark, J.; Dzulkurnain, N. A.; Hernández, G.; Mahun, A.; Abbrent, S.; Brus, J.; Kobera, L.; Edström, K. Garnet-Poly(ϵ-caprolactone- co-trimethylene carbonate) Polymer-in-Ceramic Composite Electrolyte for All-Solid-State Lithium-Ion Batteries. *ACS Applied Energy Materials* **2021**, *4* (3), 2531−2542.
(28) Sajiri, W. N. S.; Woo, H. J. Biodegradable poly (ϵ-caprolactone)/lithium bis(trifluoromethanesulfonyl) imide as gel polymer electrolyte. *Ionics* **2017**, *23* (10), 2657−2662.
(29) Karthik, K.; Murugan, R. Flexible high Li^+ conductive lithium garnet−based dry solid polymer electrolyte membrane with enhanced electrochemical performance for lithium metal batteries. *Ionics* **2019**, *25* (10), 4703−4711.
(30) Zhang, N.; He, J.; Han, W.; Wang, Y. Composite solid electrolyte PEO/SN/$LiAlO_2$ for a solid-state lithium battery. *J. Mater. Sci.* **2019**, *54*, 9603−9612.
(31) Jouault, N.; Moll, J. F.; Meng, D.; Windsor, K.; Ramcharan, S.; Kearney, C.; Kumar, S. K. Bound polymer layer in nanocomposites. *ACS Macro Lett.* **2013**, *2* (5), 371−374.
(32) Starr, F. W.; Douglas, J. F.; Meng, D.; Kumar, S. K. Bound Layers "Cloak" Nanoparticles in Strongly Interacting Polymer Nanocomposites. *ACS Nano* **2016**, *10* (12), 10960−10965.
(33) Holt, A. P.; Griffin, P. J.; Bocharova, V.; Agapov, A. L.; Imel, A. E.; Dadmun, M. D.; Sangoro, J. R.; Sokolov, A. P. Dynamics at the polymer/nanoparticle interface in poly(2-vinylpyridine)/silica nanocomposites. *Macromolecules* **2014**, *47* (5), 1837−1843.
(34) Qiao, R.; Deng, H.; Putz, K. W.; Brinson, L. C. Effect of particle agglomeration and interphase on the glass transition temperature of polymer nanocomposites. *J. Polym. Sci., Part B: Polym. Phys.* **2011**, *49* (10), 740−748.
(35) Claridge, T. D. W. In *High-Resolution NMR Techniques in Organic Chemistry*, 3rd ed.; Elsevier Science, 2016. DOI: 10.1016/C2015-0-04654-8.
(36) Rosenwinkel, M. P.; Andersson, R.; Mindemark, J.; Schönhoff, M. Coordination effects in polymer electrolytes: Fast Li+ transport by weak ion binding. *J. Phys. Chem. C* **2020**, *124* (43), 23588−23596.
(37) Xu, C.; Sun, B.; Gustafsson, T.; Edström, K.; Brandell, D.; Hahlin, M. Interface layer formation in solid polymer electrolyte lithium batteries: An XPS study. *Journal of Materials Chemistry A* **2014**, *2* (20), 7256−7264.
(38) Sångeland, C.; Hernández, G.; Brandell, D.; Younesi, R.; Hahlin, M.; Mindemark, J. Dissecting the Solid Polymer Electrolyte−Electrode Interface in the Vicinity of Electrochemical Stability Limits. *ACS Appl. Mater. Interfaces* **2022**, *14* (25), 28716−28728.
(39) Lasri, K.; Dahbi, M.; Liivat, A.; Brandell, D.; Edström, K.; Saadoune, I. Intercalation and conversion reactions in $Ni_{0.5}TiOPO_4$ Li-ion battery anode materials. *J. Power Sources* **2013**, *229*, 265−271.
(40) Kozawa, T. Combined wet milling and heat treatment in water vapor for producing amorphous to crystalline ultrafine $Li_{1.3}Al_{0.3}Ti_{1.7}(PO_4)_3$ solid electrolyte particles. *RSC Adv.* **2021**, *11* (24), 14796−14804.
(41) Kizilaslan, A.; Kirkbinar, M.; Cetinkaya, T.; Akbulut, H. Sulfur doped $Li_{1.3}Al_{0.3}Ti_{1.7}(PO_4)_3$ solid electrolytes with enhanced ionic conductivity and a reduced activation energy barrier. *Phys. Chem. Chem. Phys.* **2020**, *22* (30), 17221−17228.
(42) El Jazouli, A.; Krimi, S.; Manoun, B.; Chaminade, J. P.; Gravereau, P.; De Waal, D. Preparation and structural characterization

of two new titanium phosphates $NaCa_{0.5}Ti(PO_4)_3$ and $Ni_{0.5}TiOPO_4$. *Annales de Chimie - Science Des Matériaux* **1998**, *23* (1−2), 7−10.
(43) Jin, Y.; Liu, C.; Jia, Z.; Zong, X.; Li, D.; Fu, M.; Wei, J.; Xiong, Y. Building a highly functional $Li_{1.3}Al_{0.3}Ti_{1.7}(PO_4)_3$/poly(vinylidene fluoride) composite electrolyte for all-solid-state lithium batteries. *J. Alloys Compd.* **2021**, *874*, No. 159890.
(44) Zhou, Q.; Ma, J.; Dong, S.; Li, X.; Cui, G. Intermolecular Chemistry in Solid Polymer Electrolytes for High-Energy-Density Lithium Batteries. *Adv. Mater.* **2019**, *31* (50), 1−21.
(45) Wieczorek, W.; Stevens, J. R.; Florjańczyk, Z. Composite polyether based solid electrolytes. The Lewis acid-base approach. *Solid State Ionics* **1996**, *85* (1−4), 67−72.

https://doi.org/10.1021/acsaem.4c00701
ACS Appl. Energy Mater. 2024, 7, 4609−4619